Simulation of the Time-Dependent Flow Field in the Hypersonic Ludwieg Tube Braunschweig

Torsten Wolf, Malte Estorf and Rolf Radespiel

Technical University Braunschweig, Institute of Fluid Mechanics, Bienroder Weg 3, D-38106 Braunschweig, Germany

E-Mail: t.wolf@tu-bs.de

Abstract

In summer 2003 the Hypersonic Ludwieg Tube Braunschweig (HLB) has been commissioned. It has been designed for a Mach number $M = 6$. The operative range of the unit Reynolds number is between $3 \cdot 10^6$ 1/m and $20 \cdot 10^6$ 1/m. The test section has a diameter of 500 mm and the run time with near steady flow conditions is 80 ms. The intermittent working principle implies an unsteady onset of the flow with considerable influence on the flow quantities in the test section. In this paper we describe the attempt to simulate the time-dependent flow in the HLB. Foregoing simulations and test cases are discussed. The framework of the time-dependent simulations is described. We present first results of the unsteady, inviscid flow field in the HLB including the opening of the valve and compare them with experimental data.

Nomenclature

d	distance
d^*	diameter in the nozzle throat
l	reference length
M	Mach number
p	pressure
ϱ	density
Re	Reynolds number
t	time
T	temperature
x, z	global coordinates
X, Z	coordinates in the test section

Subscripts

pit	quantity behind a normal shock
s	shock wave
tot	total quantity
vac	initial quantity in vacuum section
1	behind expansion wave in the tube

1 Introduction

Aerothermal design of reusable reentry vehicles requires good knowledge of aerodynamic and thermal loads on all structural components. Although numerical methods for hypersonic flow simulations are already well developed the experimental proof is still essential. Because of their low operational cost and good flow quality Ludwieg tube type cold blow-down tunnels are of special interest. They need no total pressure control device or large settling chamber as conventional blow-down facilities. The operational effort for Ludwieg-type tunnels can be further reduced by the use of a fast acting valve instead of the bursting diaphragm originally suggested by Ludwieg [1]. The development of a Ludwieg tube with such a valve in the throat of the hypersonic nozzle is documented in [2]. According to the facility described there a new hypersonic wind tunnel has been built and commissioned at the Institute of Fluid Mechanics in Braunschweig over the last two years. During the design of the hypersonic nozzle extensive Navier-Stokes calculations were conducted in order to optimize the contour of the nozzle throat and the straightening section considering the displacement thickness of turbulent nozzle wall boundary layers. With an optimized nozzle contour the non-uniformity in pitot pressure within the test section due to the wake of the valve turned out to have the same magnitude as the remaining non-uniformities due to the expansion and compression waves from the nozzle. First measurements of the pitot pressure in the test section have been presented in [3] and [4]. They showed a deviation of about $\pm 1.2\%$ over a vertical transverse through the test section. A temperature stratification in the wind tunnel was also discovered.

The flow entering the test section of the HLB differs from an ideal inflow as it would be the case in the atmosphere. These deviations are of principal nature and partially intended. They fall into two categories, namely geometric and time-dependent deviations.

Geometric deviations: This type of deviations results from the geometry of the HLB nozzle and the presence of the valve body on the symmetry axis. In radial direction they appear as non-uniformities in the flow quantities forming a wake in the vicinity of the symmetry axis. Some flow expansion along the test section also belongs to this category. These deviations would also appear in steady flow and have been examined extensively in the past.

Time-dependent deviations: Due to the intermittent working principle of the HLB the onset of the flow is time-dependent, beginning with the opening of the valve and the developement of the hypersonic flow. This is followed by a timeframe with near-steady flow conditions and finally the breakdown of flow after closure of the valve.

In order to interpret the results of experiments in the HLB, the magnitude and influence of these deviations

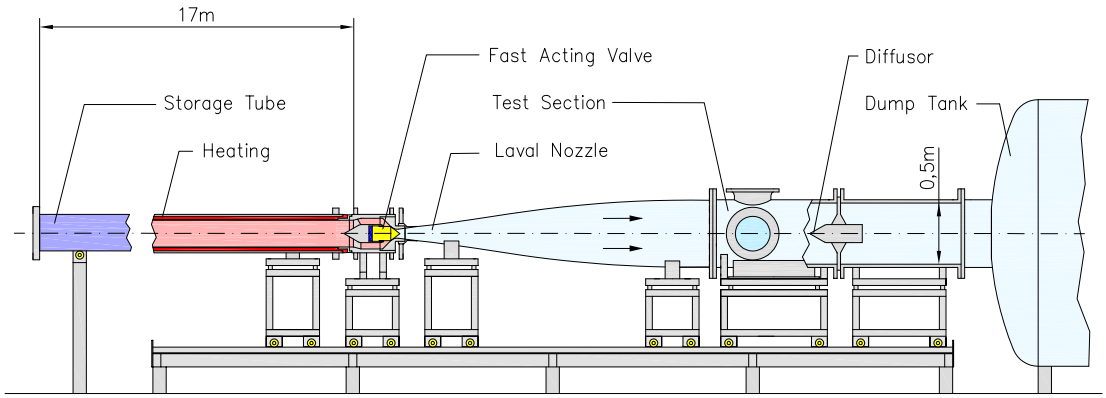

Figure 1: Sketch of the HLB

has to be known so that the measured data can be corrected. One way to gather this knowledge is to rebuild the time-dependent flow field in the HLB with numerical methods. With the results of this rebuilding, time-dependent simulations of the flow around test objects in the HLB can be conducted and then be compared to simulations with nominal test conditions. Such simulations including the opening process of the valve require a large computational effort to resolve the fast flow interactions during the onset of flow and to simulate the – compared to the size of the physical time step – very long run time and opening time.

This paper outlines the efforts made, to simulate the time-dependent flow in the HLB. First, we describe the test facility and show results of simulations of the steady flow in the HLB. We describe the preliminaries of the numerical rebuilding which consist of determing optimal solver settings and exploring the influence of temporal and spatial discretisation. The framework of the simulations including the valve opening is presented. We show results of the time-dependent flow field in the HLB with major simplifications like neglecting the valve and finally the first results for the HLB employing the opening process. Comparisons with experimental data help to evaluate the success of these first simulations.

2 Facility Description

2.1 Working Principle

A schematic diagram of the HLB is given in Fig. 1. The assembly is divided into a high pressure and a low pressure section, which are separated by a fast acting valve. The high pressure section consisting of the 17 m long storage tube with a 3 m long heated section can be pressurized to up to 30 bar. The low pressure section comprising the hypersonic nozzle, the test section, the diffusor and a 6 m^3 dump tank is evacuated before each run to about 1 mbar. The heating to up to 600 K is necessary to prevent condensation effects of the gas during the expansion in the hypersonic nozzle. The valve basically consists of a pneumatically driven piston which fits into the nozzle throat with its conical end (cf. Fig. 2). The valve can be opened for about 100 ms. This causes an expansion wave to run into the storage tube. Across the wave the air is accelerated towards the nozzle where it is further expanded up to $M = 5.9$ in the test section. The expansion wave traveling through the storage tube is reflected at its end and reaches the valve again after about 90 ms. This is the timeframe of near steady flow conditions in the test section. The closure of the valve inhibits complete equalisation of pressure in the facility, which saves energy and time.

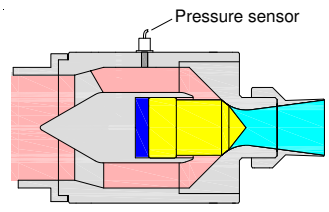

Figure 2: HLB valve in closed end position

Fig. 2 additionally shows the driver tube pressure sensor which is located in the valve section 200 mm upstream of the nozzle throat. The variation of pressure in time recorded by this sensor is used for comparisons with numerical simulations.

2.2 Steady Flow

The steady flow field in the HLB has been examined extensively in the past. RANS calculations were used to improve the initial nozzle design which showed distinct compression and expansion waves (cf. Fig. 3, top). Simulations taking the boundary layer displacement thickness into account and variations of the nozzle contour led to

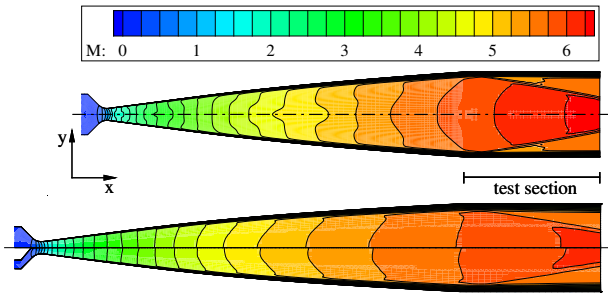

Figure 3: Calculated steady Mach number distribution in a nozzle with preliminary design (upper) and in the final design nozzle (lower). The latter with and without valve body in the lower and upper nozzle half respectively.

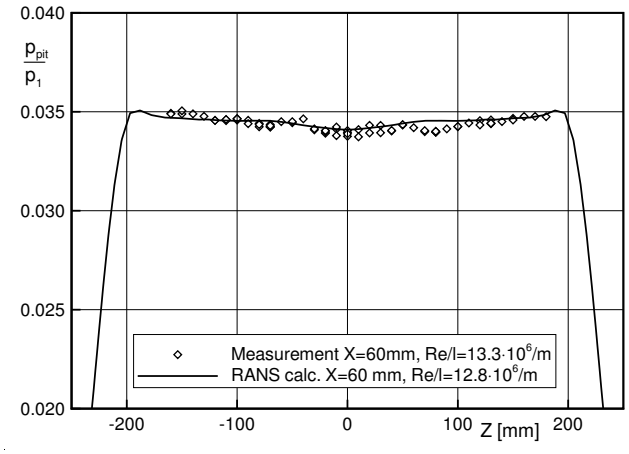

Figure 4: Measured pitot pressures compared to RANS calculation of the steady flow in the HLB

the improved design (for details see [5]). The resulting nozzle design is shown in Fig. 3 (bottom). The Mach number distribution shows a smooth expansion of the flow and a near constant distribution in the test section. For the final design the influence of the valve body on the symmetry axis has been examined. The wake of the valve body can be seen in Fig. 3. However, the influence of the valve on the non-uniformity in the test section is about the same as the remaining non-uniformity in the simulation without the valve. The Mach number distributions also show an expansion of the flow in the test section which is imposed to make the flow less sensitive to deviations from the design point.

The distribution of the pitot pressure across the test section at a position 60 mm downstream of the test sectional entry plane shown in Fig. 4 is almost constant. Additionally, the measured pressures are in good agreement with RANS calculations of the steady flow in the HLB nozzle.

The valve body is located in the heated section of the wind tunnel while the outer hull of the tunnel has ambient temperature. Therefore, a temperature wake develops near the symmetry axis of the wind tunnel. RANS calculations of the steady flow in the HLB show a distinct

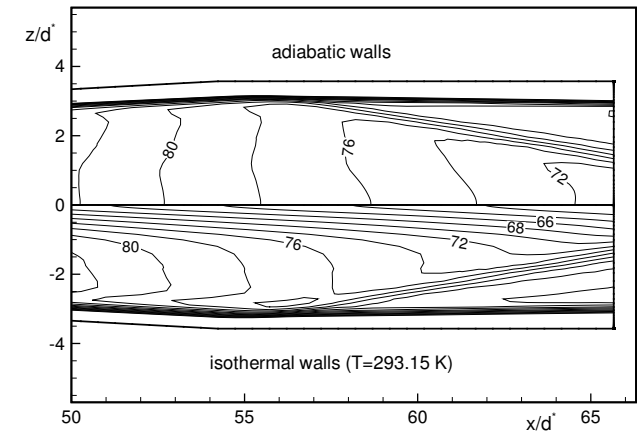

Figure 5: Temperature distributions (K) in the test section in steady flow for different boundary conditions, $p_{tot} = 20\,\mathrm{bar}$

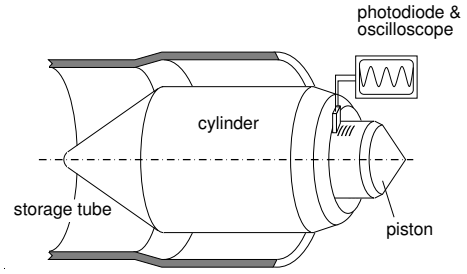

Figure 6: Schematic measurement setup for valve opening

wake in case of isothermal walls with all wall temperatures equal to the ambient temperature. In Fig. 5 this result is compared with adiabatic walls. In the latter case the wake results solely from the expansion in the test section. However, information how fast such wakes develop and thus influence the heating of a model in the test section can only be provided by time-dependent calculations.

2.3 Valve Opening

The speed of the valve is an essential input parameter for the numerical simulation of the flow inside the HLB. The experimental setup for measuring the opening is shown in Fig. 6. A photodiode is attached to the front of the valve body while a foil with a pattern of alternating black and white lines is put on the side of the piston. The width of the lines is 1 mm. The alternating voltage signal of the photoelectric relay during opening and closure is recorded by an oscilloscope. The measurement is triggered by the valve-control. The resulting variation of voltage in time shows a speed of the piston of $5\,\mathrm{m/s}$. The traverse path is about 48.5 mm which is in agreement with the manufacture drawings. These measurements have also revealed an undesireable behaviour of the piston movement. The original settings of the valve control lead to a blockage in the pneumatics so that the piston stops on its path, reverses its direction for a short way and finally covers the remaining traverse path. With modified settings this behaviour has almost completely been corrected. The piston speed stated above has been measured with the corrected settings.

3 Numerical Simulations

3.1 The DLR TAU-Code

The TAU-Code developed at DLR [6] discretises the Reynolds-averaged Navier-Stokes equations by a finite-volume technique on hybrid grids and has been validated for hypersonic flows in [7]. Acceleration techniques such as multigrid and residual smoothing are available. For the simulations presented in this paper a dual-time stepping approach with an LU-SGS algorithm for the inner iterations is chosen. Fluxes are calculated second-order accurate, assuming an ideal gas. The TAU-Code uses the self-describing NetCDF format for grid and solution files, thus enabling the user to easily access and modify variables and attributes.

The grids used in the simulations in this paper are 2D and created with CENTAUR [8]. For simulations of the flow in the HLB, the 2D grids are converted to an axisymmetric format, thus representing a segment of the complete 3D rotationally symmetric wind tunnel. The opening angle is 3°. This allows for faster solver operation, increased accuracy near the axisymmetry axis and less points compared to a full 3D computation.

In the preliminary stages of the simulation of the flow in the HLB several test cases are considered helping to determine solver settings suited for this type of problem.

3.2 Solver Settings

3.2.1 Calculation of Convective Fluxes

Special care has been taken to choose an appropriate scheme for the calculation of the convective fluxes across a control volume with respect to accuracy, stability in presence of strong shocks and numerical effort. The schemes examined are the approximate Riemann solvers of Roe and HLLE and flux vector splitting methods of the CUSP-, the AUSM- and the AUFS-family and MAPS+ (cf. [9], [10], [11], [12], [13] and [14]). The test cases considered are a stationary normal shock, shock reflection on a wedge and Sod's shock tube problem.

Stationary normal shock: This 2D test case is used to examine the robustness and the accuracy of the different upwind schemes. For a set of chosen flow quantities and a Mach number of $M = 20$ upstream of the shock, the quantities downstream are determined by the Rankine-Hugionot relations. On a rectangular mesh a one-cell wide disturbed region was created by prescribing the arithmetic mean values of the left and right state. Fig. 7 shows the computed density distributions across the shock for selected upwind schemes. Best results are obtained with the AUSMPW+ scheme [15] (one inner point) and a combination of the H-CUSP and the HLLE scheme (no inner point). For the latter, the very dissipative yet robust HLLE scheme replaces the H-CUSP scheme at discontinuities. AUSMDV and AUFS exhibit more inner points and are therefore undesireable. The

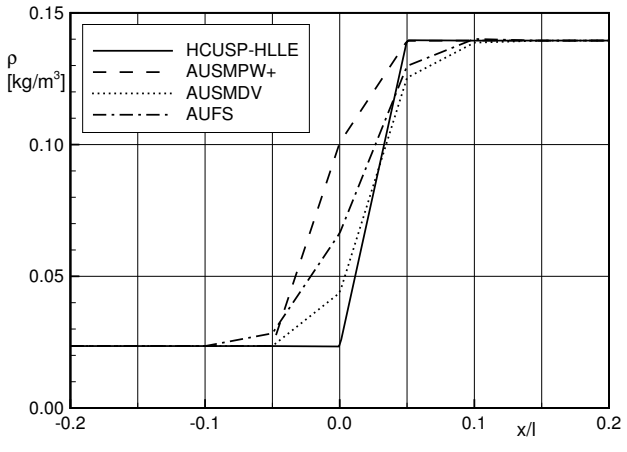

Figure 7: Density distributions across a stationary normal shock ($M = 20$) for different upwind schemes

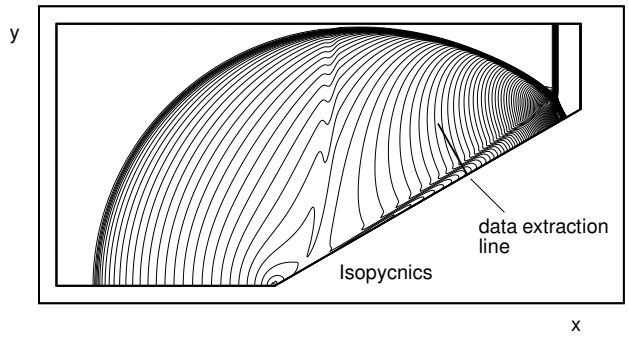

Figure 8: Shock reflection at a 30° wedge, $M_s = 1.2$; density distribution

Roe scheme even with entropy fix fails, thus no results are shown.

Single Mach reflection: This instationary test case serves to reveal the dissipation of each scheme. The case described in [16] comprises a wedge with an angle of 30° and an incident weak shock with a shock wave Mach number $M_s = 1.2$. The resulting reflection is a so called single Mach reflection (SMR, cf. [17]). The difficulty for the flux scheme lies in resolving the shear layer emanating from the triple point, visible in the exemplary density distribution in Fig. 8. The underlying reference grid consists of 512 points in streamwise direction and 256 points in vertical direction. A coarser grid (200×96) is used for the scheme comparisons. The performance of various schemes is displayed in the density distributions along a line normal to the wedge, shown in Fig. 9. At some distance from the wall, the three schemes give similar results. However, at the wall only AUSMPW+ shows a clear tendency towards the solution obtained on the finer reference grid with a much crisper shear layer.

Sod's shock tube: The last test case intends to determine which scheme is most suitable for moving discontinuities such as shocks and contacts. A 2D rectangular grid is used and the left and right states are similar to the conditions in the HLB. The pressure upstream of the initial discontinuitiy is 10 bar and 1 mbar downstream, while the temperature in both regimes is 293.15 K. The

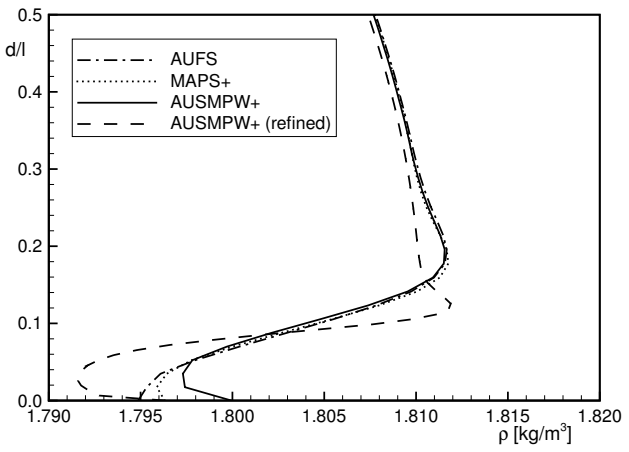

Figure 9: Density distribution in wall-normal direction for different upwind schemes

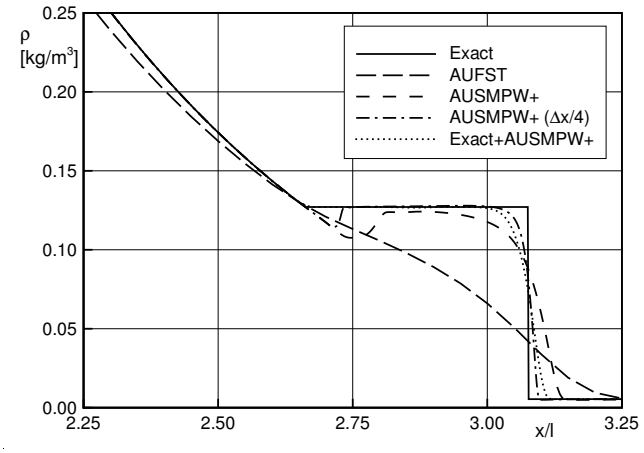

Figure 10: Density distribution for Sod's shock tube; expansion wave and contact discontinuity

air is assumed to be a perfect and inviscid gas. Results of the different schemes are compared with the exact solution of this problem. We chose the AUSMPW+ scheme which performed best in the aforementioned test cases. The AUFS scheme serves as an example of worse performance. Fig. 10 shows the density distributions at the end of the expansion wave and across the contact discontinuity. While AUFS smears the contact, AUSMPW+ matches the exact solution quite well. However, there exists a glitch right at the end of the expansion which becomes smaller if the grid spacing in streamwise direction is quartered. This error arises when starting the solution from an initial discontinuity and vanishes when restarting from the exact solution. Fig. 11 shows the density distributions across the shock. It can be seen that a calculation on the given grid using the exact solution as a start condition matches the exact distribution as good as a simulation on a grid four times finer but being initiated from a discontinuity.

3.2.2 Discretisation Error

With the AUSMPW+ scheme performing best in the previous test cases, a simple 2D Ludwieg tube is used to examine the influence of the spatial discretization. This generic windtunnel consists of a short storage tube and

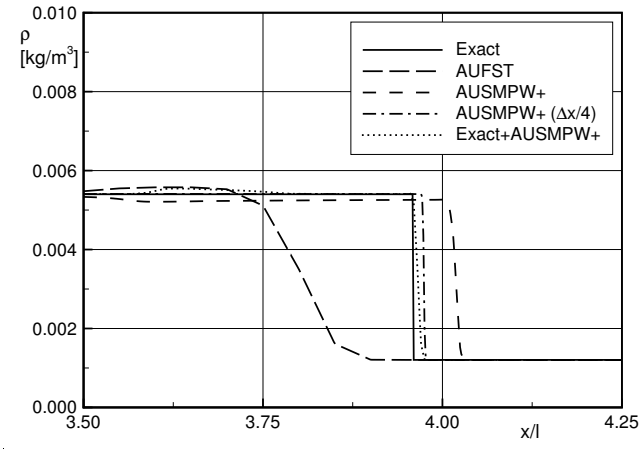

Figure 11: Density distribution for Sod's shock tube; shock discontinuity

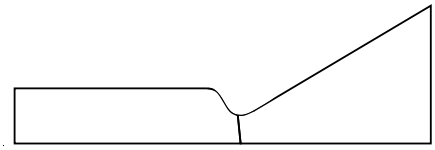

Figure 12: Geometry of the generic wind tunnel

a conical nozzle and is shown in Fig. 12. A membrane is located upstream, near the nozzle throat and divides the storage tube from the nozzle. The initial conditions are similar to those in the HLB, namely $p_{tot} = 10\,\mathrm{bar}$, $T_{tot} = 600\,\mathrm{K}$, $p_{vac} = 1\,\mathrm{mbar}$ and $T_{vac} = 295\,\mathrm{K}$. A structured mesh is used with 128 cells in radial and 700 cells in streamwise direction. During the study this mesh is refined in streamwise direction twice, each time doubling the number of cells. The size of the physical time step is chosen to maintain stability of the simulation and to resolve the development of the flow adequately. Fig. 13 shows the variation of temperature and pressure in time recorded at the exit of the nozzle at the symmetry axis of the windtunnel. Seven milliseconds after the flow initialisation, the hot gas slug between the foremost shock wave and the following contact discontinuity exits the nozzle. As one can easily see, the influence of the grid spacing in streamwise direction is restricted to the resolution of this slug. During the afterward operation of the windtunnel, all three solutions are virtually identical. If the hot slug is of minor interest the grid density can be kept within moderate bounds.

3.3 Simulation Framework with Valve Opening

The simulation of the flow in the HLB including the opening of the valve is carried out in the following manner. An initial grid with a slightly opened valve is created. The gap between the piston and the nozzle throat must be wide enough so that it can be discretised by an appropriate amount of cell layers. On the other hand, the gap should be as small as possible to allow almost full simulation of the piston movement. With a traverse path of 50 mm the initial gap width in the following simulations is about 0.61 mm. The states in the pressurized

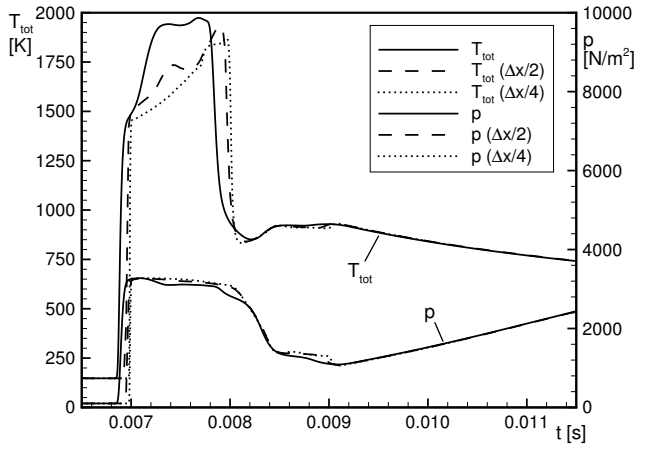

Figure 13: Variation of total temperature and pressure at nozzle exit in time for simple 2D-Ludwieg tube

and the vacuum part are imposed onto a restart file. A virtual membrane is located where the gap between the valve and the nozzle throat is most narrow. After the calculation of one unsteady time step, the primary grid is deformed by moving the piston contour by the product of the timestepsize and the piston speed. Then the TAU preprocessor creates the secondary grid so that the following time step can be calculated and so on.

3.3.1 Solution Migration

Grid deformation cannot be carried out arbitrarily long, as the cells near the piston become increasingly skewed, and this increases the discretisation error. Therefore, the whole traverse path is divided into segments. Each segment starts with an initial grid and is covered via deformation. At the junction of two consecutive segments, the solution has to migrate to the next initial grid. The TAU-Code does not provide a tool for migration of a solution between two grids with identical boundaries, so a routine has been developed using MPI to allow parallel execution. The interpolation method is quite simple and calculates an inverse distance weighted interpolant (the number of considered neighbours can be prescribed). In case the next point lies within a very small distance, the value is simply copied. This method has proven to be very effective, robust and accurate enough. Fig. 14 shows the density error in percent of the absolute density after two interpolations. It can be seen, that the error in smooth regions is less than 0.1 % and reaches values of about 5% only at shocks. No further effort was put into decreasing the error around discontinuites as such deviations usually smear during the progress of the simulation.

3.3.2 Grid Deformation

The deformation routine of the original TAU-Code has two drawbacks. It runs sequentially and gives poor results when being applied to the grids in this project. Thus, a new deformation routine using MPI has been developed. The routine takes information about the deformed boundary markers and the type of deformation

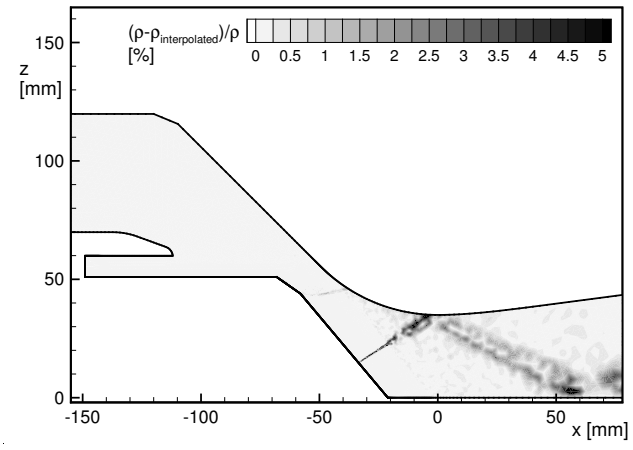

Figure 14: Error in density distributions after two solution migrations

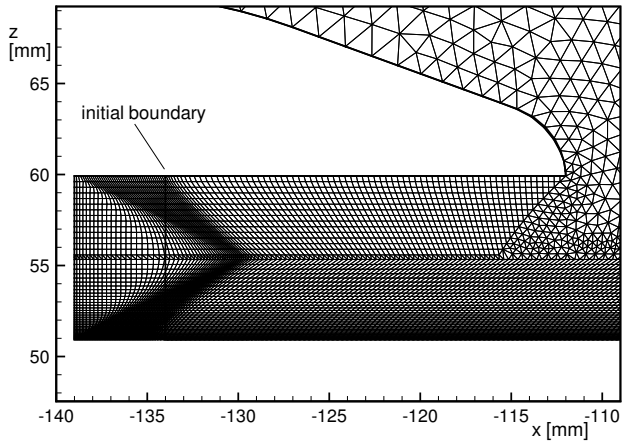

Figure 15: Deformed grid in the gap between valve body and piston; deformation way $\Delta x = 5\,\mathrm{mm}$

(stretching and translation) as input and modifies the grid file accordingly. Grid points in the vicinity of deformed boundaries within a given wall distance are displaced by the amount the nearest boundary point moves, scaled with the distance between them. Several scaling functions are available, allowing the user to choose a scaling best suited for the current problem. Fig. 15 shows an exemplary grid of the gap between fixed and moving parts of the valve in its last deformation stage, just before the solution would migrate to the successor grid. The initial boundary gives an impression how far the grid can be stretched. The whole traverse path can be covered within 10 migration steps.

3.4 Simulation Program

3.4.1 Simplified Geometry without Valve

Two different HLB geometries are examined. First results are obtained for a simplified geometry without modeling the movement of the piston (cf. Fig. 16, upper half). The valve is open during the whole simulation. At startup the pressurized and the vacuum regime are separated by a membrane (also visible in Fig. 16). The initial conditions are $p_{tot} = 20\,\mathrm{bar}$, $p_{vac} = 1\,\mathrm{mbar}$, $T_{tot} = 600\,\mathrm{K}$ and $T_{vac} = 295\,\mathrm{K}$. In both regimes the initital velocity is zero and air is assumed to be perfect and inviscid. The grid is 2D axisymmetric as described in section 3.1. There are 64 grid points in radial and 740 grid points in axial direction. The physical timestepsize is $\Delta t = 5 \cdot 10^{-8}\,\mathrm{s}$. The simulation runs for 23 ms.

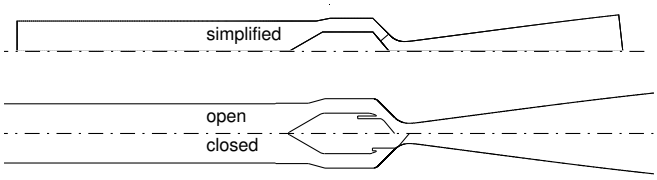

Figure 16: Simplified and full HLB contours

3.4.2 HLB Geometry with Valve

This geometry features piston movement that is neglected in the previous simulation. The valve position varies between near closure with the initial gap mentioned in section 3.3 and the opened state. The initial conditions are the same as for the simplified geometry. During the first unsteady time steps, the width of the physical time step has to be decreased from $\Delta t = 5 \cdot 10^{-8}\,\mathrm{s}$ to $\Delta t = 5 \cdot 10^{-9}\,\mathrm{s}$ due to stability issues. The number of points varies from 125 000 (valve closed) to 168 000 points (valve opened).

On an SMP-System (IBM p690 Regatta, 1.3 GHz) the simulation of 20 ms using 6-8 CPUs takes about 100 days. This effort has to be reduced, especially when including viscous effects. One possible acceleration is to shorten the simulation by increasing the piston speed. The basic idea is, that the speed of the valve is much smaller than the speed at which information is passed through the flow field, e.g. when adapting to geometry changes. Thus, it is being examined if the valve speed could be artifically increased and the results stretched in time accordingly. Therefore, an additional simulation with a piston speed of $20\,\mathrm{m/s}$ is performed.

4 Results

4.1 Simplified Geometry

With the membrane vanishing an expansion wave travels into the storage tube and a shock and a contact discontinuity run towards the nozzle throat. A shock develops at the tip of the piston and bends the flow away from the symmetry axis so that it runs into the nozzle. Numerous compression waves travel from the throat towards the storage tube until the flow calms down and becomes near steady.

The variation of the static pressure in time at the driver tube pressure sensor in the valve section is recorded and compared with a measured pressure distribution in Fig. 17. As the total pressures differ (20 bar in the simulation and 15 bar in the experiment), both variations are made dimensionless with the respective total pressure. It can be clearly seen, that the onset of flow in the simulation is too sudden. Furthermore, the transition to a smooth, near steady flow is completed too fast. This leads to the conclusion, that without the opening process of the valve the onset of flow cannot be rebuilt properly. The high frequent oscillations visible in the numerical pressure history are damped very slowly. Note that viscous effects are neglected in this simulation.

4.2 HLB Geometry with Valve Opening

At the beginning of the simulation, the flow in the gap between the valve piston and the nozzle contour starts in the manner of the Riemann problem, i.e. an expansion fan travels towards the valve body and a shockwave and contact discontinuity run into the nozzle. Again, an oblique shock develops at the tip of the piston where the flow has to turn parallel to the symmetry axis. This shock is reflected multiple times at the nozzle contour

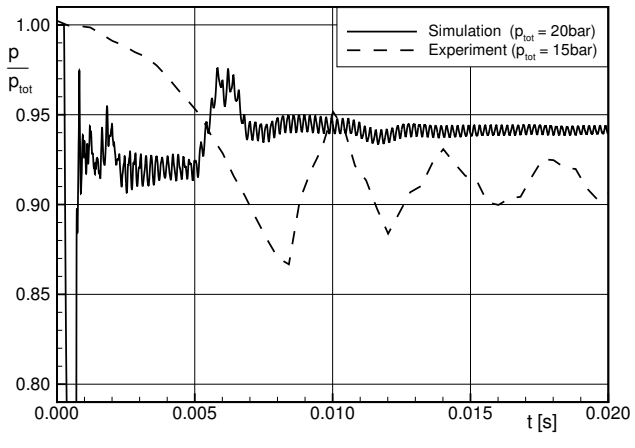

Figure 17: Variation of pressure in time for simulations and experiment for the simplified HLB geometry without valve opening

and the symmetry axis downstream, until the flow is parallel to the axisymmetry axis in the test section. Within the gap between piston and valve body the sudden movement of the piston induces an expansion wave, which travels through the gap and is refracted at the front of the valve body. During the opening, the flow is subsonic along the cylindrical part of the piston until the kink at the front of the piston. There an expansion fan develops and the flow becomes supersonic. This fan is visible in Fig. 18 at $t = 1\,\mathrm{ms}$ and is marked by 'EX'. As a 3D effect the streamlines are condensed while running towards the tip of the piston. Thus, a compression wave develops and is reflected at the nozzle contour at the location marked by 'R'. With the gap between the piston and the nozzle throat widening, the expansion fan becomes weaker and the oblique shock at the piston tip travels upstream ($t = 1.35\,\mathrm{ms}$). Behind the shock, the sonic line is about to relocate towards the nozzle throat. As the piston moves further, the reflected compression wave steepens and finally vanishes ($t = 1.5\,\mathrm{ms}$). At this point, the flow around the piston becomes completely subsonic and the remainder of the oblique shock runs as a compression wave into the storage tube ($t = 1.85\,\mathrm{ms}$).

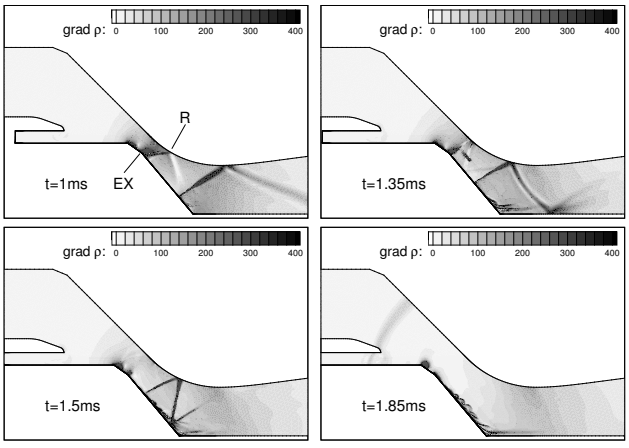

Figure 18: Development of the flow in the vicinity of the valve; schlierenpictures at different times for fast moving valve

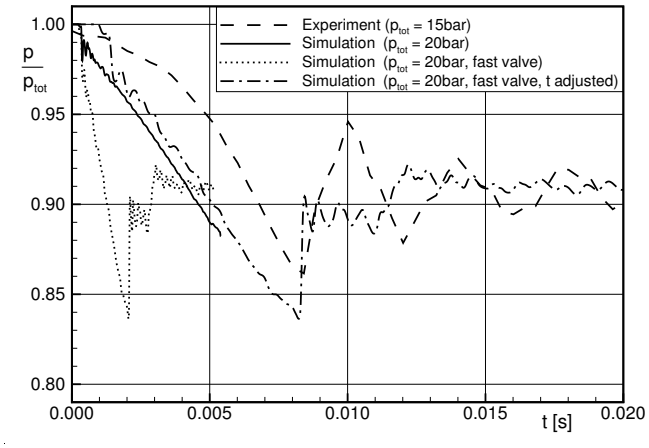

Figure 19: Variation of pressure in time for simulations and experiment

Finally, when the piston comes to rest at the end of the traverse path compression waves emanate from the tip and within the gap. From now on, the flow becomes smooth, while vortices and flow separations at the piston vanish and are convected through the nozzle throat.

4.2.1 Valve speed 5 m/s

In Fig. 19 the variation of pressure is compared with experimental data. Unfortunately, the computation is still ongoing work but the pressure variation in Fig. 19 calculated up to now shows a decrease rate similar to the measured one. Note that the valve in the experiments does not exhibit a sudden movement but is accelerated smoothly from rest to the speed of 5 m/s. Hence the deviations seem reasonable.

4.2.2 Valve speed 20 m/s

Fig. 19 shows the pressure variation in case of the fast valve commonly scaled and stretched by a factor of four. It can be seen, that the decrease in pressure happens at nearly the same rate for both valve speeds. Even more remarkable is that the pressure rise in the simulation of the fast valve after 8 ms nicely matches the measured one. The temporal discretisation of the numerical simulation is at least two orders of magnitude finer than the pressure sensors, thus high-frequent oscillations are calculated that do not show up in the measurements. When the valve is fully open the calculated and the measured pressures are nearly the same. However, this approach needs more validation before it can be applied to future simulations.

5 Concluding Remarks

The Hypersonic Ludwieg Tube at Braunschweig is a facility with remarkable low operational cost. Initial difficulties such as temperature stratification in the windtunnel and an irregular piston movement behaviour have been overcome. The measured pitot distributions in the test section show a good uniformity and the Mach number at the location of test objects is constant $M = 5.9$.

In order to determine the deviations from nominal test conditions due to the intermittent working principle of the wind tunnel, a numerical rebuilding of the time-dependent flow in the HLB is investigated. The difficulty in this task is the difference between the timescales of the valve opening and the propagation of disturbances in the flow. Thus, the width of the time step is very small compared to the opening time of the valve. Accompanying test cases are used to choose an appropriate scheme for the convective fluxes and to adjust the solver settings. First simulations of the HLB without the valve opening and a simplified geometry predict an onset of flow which is too sudden compared to measurements. Simulations of the flow in the HLB including the valve opening are presented and show a correct tendency towards experimental data. Due to the enormous computational effort a simulation with a valve piston speed four times higher than the original was also conducted. The results – stretched by a factor of four – are in good agreement with the simulations at the original speed as well with measured data. It will be examined in the future if this approach to accelerate the simulation program is valid.

Future tasks are the incorporation of viscous effects to obtain more realistic results in regions of flow separation e.g. at the piston.

References

[1] H. Ludwieg, *Der Rohrwindkanal*, Z. f. Flugwiss. 3, Nr. 7, (1955) pp. 206–216.

[2] G. Koppenwallner, R. Müller-Eigner, H. Friehmelt, *HHK Hochschul-Hyperschall-Kanal: Ein 'Low-Cost' Windkanal für Forschung und Ausbildung*, DGLR Jahrbuch, Band II (1993).

[3] M. Estorf, R. Radespiel, M. Heine, R. Müller-Eigner, *Der Hyperschallwindkanal Ludwiegrohr Braunschweig HLB*, in *DGLR-Jahrbuch 2003* (2003), Vol. 1, pp. 661–670.

[4] M. Estorf, T. Wolf, R. Radespiel, *Experimental and numerical investigations on the operation of the Hypersonic Ludwieg Tube Braunschweig*, 5th European Symposium on Aerothermodynamics for Space Vehicles (2004).

[5] D. Kožulović, R. Radespiel, R. Müller-Eigner, *Aerodynamic design parameters of a hypersonic Ludwieg tube nozzle*, in D. Z. et al., (Eds.) *Proceedings of the West East High Speed Flow Fields Conference*, CIMNE, Barcelona, Spain (2002).

[6] *Technical Documentation of the DLR TAU-Code*, DLR (2004).

[7] A. Mack, V. Hannemann, *Validation of the Unstructured DLR-TAU-Code for Hypersonic Flows*, AIAA Paper 2002-3111 (2002).

[8] *Centaur* (2004), `http://www.centaursoft.com`.

[9] P. L. Roe, *Approximate Riemann Solvers, Parameter Vectors and Difference Schemes*, Journal of

Computational Physics, Vol. 43, (1981) pp. 357–372.

[10] B. Einfeldt, *On Godunov-type methods for gas dynamics*, SIAM J. Numer. Anal., Vol. 25, (1988) pp. 294–318.

[11] S. Tatsumi, L. Martinelli, A. Jameson, *A New High Resolution Scheme for Compressible Viscous Flow with Shocks*, AIAA Paper 95-0466 (1995).

[12] M.-S. Liou, *Ten Years in the Making - AUSM-family*, AIAA Paper 2001-2521 (2001).

[13] M. Sun, K. Takayama, *An artificially upstream flux vector splitting scheme for the Euler equations*, Journal of Computational Physics, Vol. 189, (2003) pp. 305–329.

[14] C.-C. Rossow, *A Flux Splitting Scheme for Compressible and Incompressible Flows*, Journal of Computational Physics, Vol. 164, (2000) pp. 104–122.

[15] K. H. Kim, C. K. Kim, O.-H. Rho, *Methods for the Accurate Computations of Hypersonic Flows*, Journal of Computational Physics, Vol. 174, (2001) pp. 38–80.

[16] E. F. Toro, *Riemann Solvers and Numerical Methods for Fluid Dynamics*, Springer-Verlag, Berlin Heidelberg, 2nd Edition (1999).

[17] G. Ben-Dor, *Shock Wave Reflection Phenomena*, Springer-Verlag, New York (1992).